Polymer 162 (2019) 130–138

Contents lists available at ScienceDirect

Polymer

journal homepage: www.elsevier.com/locate/polymer

Facile synthesis of coral-like hierarchical polyaniline micro/nanostructures with enhanced supercapacitance and adsorption performance

Wei Lyu[a], Mengting Yu[a], Jiangtao Feng[a,*], Wei Yan[a,b,**]

[a] Department of Environmental Science and Engineering, Xi'an Jiaotong University, 710049, Xi'an, China
[b] State Key Laboratory of Multiphase Flow in Power Engineering, Xi'an Jiaotong University, 710049, Xi'an, China

HIGHLIGHTS

- A newly facile approach is developed to scalable synthesize 3D PANI (CL-PANI).
- A possible formation mechanism and evolution process of CL-PANI is proposed.
- CL-PANI possesses unique mesoporous structure and better crystallinity.
- CL-PANI shows enhanced supercapacitance and adsorption performance.

ARTICLE INFO

Keywords:
Polyaniline
Coral-like hierarchical structure
Mesoporous structure
Supercapacitor
Adsorption

ABSTRACT

We presented a newly facile approach to scalable synthesize three-dimensional (3D) coral-like polyaniline (CL-PANI) hierarchical micro/nanostructures. The CL-PANI composed of well-defined nanowires with ca.20 nm was self-assembled *by in situ* conventional chemical polymerization with a different charging sequence. Electron microscopy, UV-Vis spectroscopy, X-ray diffraction, and nitrogen adsorption-desorption studies showed that CL-PANI possessed unique mesoporous structure and highly crystallinity which could promote rapid ion diffusion and charge transfer. Electrochemical experimental results showed that the as-prepared CL-PANI electrode had a superior electrochemical capacitance performance with a relatively high specific capacitance of 817 F g^{-1} at a current density of 0.5 A g^{-1} and a great rate capability of 67% specific capacitance retaining from 0.5 to 20 A g^{-1}. Meanwhile, CL-PANI exhibited an enhanced adsorption performance of azo dye Acid Red G (ARG) from aqueous solution with a Langmuir maximum adsorption of 310.2 mg g^{-1} at pH 2.0, 298 K. This study offers a simple and cost effective path for scalable synthesis of PANI materials for supercapacitor and adsorption application.Abstracts.

1. Introduction

Polyaniline (PANI) has been demonstrated to be a conducting polymer with incredible promise in many fields ranging from sensors [1], electrode material for batteries [2], light-emitting and electronic devices [3], anticorrosion coatings [4] to adsorbent for environmental pollutants [5]. It has the advantages of low cost, easy synthesis, unique reversible doping-dedoping electrochemical property, good environmental stability and so on [6]. During the past decade, many efforts have been made on the formation of well-defined micro/nanostructured PANI due to its higher surface area, increased processability and improved performance [7,8].

Three-dimensional (3D) hierarchical micro/nanostructures consisting of one dimensional nanowires, nanorods and other nanostructures have been demonstrated to have the merits of well-defined and accessible mesoporous, plenty surface active sites, large surface area, and enhanced structural stability and so on [9]. 3D hierarchical PANI micro/nanostructures have been synthesized with the aid of soft template or specific structure-directing agents or under extreme condition like frozen and high acid concentration [10,11]. Zhu et al. [12] prepared 3D dandelion-like PANI microstructures *via* a self-assembly process from 1D nanofibers with perfluorosebacic acid dopant served as a "soft" template. Zhou et al. [13] synthesized 3D microspheres self-assembled from nanowires in the 5.0 M H_2SO_4 aqueous solution. Wang et al. [14] synthesized a 3D hierarchical micro/nanostructured PANI using the regular dilute polymerization in the frozen and high ionic

* Corresponding author.
** Corresponding authors. Department of Environmental Science and Engineering, Xi'an Jiaotong University, 710049, Xi'an, China.
E-mail addresses: fjtes@xjtu.edu.cn (J. Feng), yanwei@xjtu.edu.cn (W. Yan).

https://doi.org/10.1016/j.polymer.2018.12.037
Received 22 June 2018; Received in revised form 28 November 2018; Accepted 24 December 2018
Available online 27 December 2018
0032-3861/

strength condition. However, the adoption of expensive specific structure-directing dopants or extreme conditions makes these 3D hierarchical micro/nanostructured PANI unsuitable for large scale applications. From a practical standpoint, developing a cost-effective, mild and high yield synthesis method without using expensive reagents and extreme condition remains a challenge for PANI's large-scale applications.

In the template-free method, suppressing the reaction kinetics plays the curial role in the formation of 3D hierarchical PANI superstructure [14], which can be achieved by adding inorganic salts as additives [15], lowering the reaction temperature [16], and diluting the concentration [17] and so on. Mazzone et al. showed that concentration gradient could suppress the homogeneous and heterogeneous nucleation process of NiZr by limiting atomic mobility [18]. Therefore, one possible way to suppress the reaction kinetics for forming 3D PANI superstructure is to generate concentration gradient of active aniline, i.e. protonated aniline, to limit its mobility during the polymerization induced period. Here, we propose a simple and low-cost way to scalable synthesize 3D coral-like hierarchical PANI micro/nanostructures in the conventional chemical polymerization process by only adjusting the charge sequence to create possible concentration gradient of protonated aniline at 0 °C.

To the best of our knowledge, only one study had reported the application of 3D PANI obtained under extreme condition in the supercapacitor area, where the 3D micro/nanostructured PANI presented an enhanced supercapacitance performance than the common one [14]. It is therefore desirable to know the supercapacitance performance of 3D coral-like hierarchical PANI prepared in this paper. Moreover, different micro/nanostructured conducting polymers had been used as adsorbents for the removal of environmental pollutants like dyes and heavy metals and showed efficient adsorption performances [19–24]. However, the adsorption performance of this 3D micro/nanostructured PANI on pollutants has not been explored extensively. And PANI with 3D micro/nanostructure is expected to show enhanced performance due to its well-defined and accessible mesoporous and plenty surface active sites.

In this paper, a low-cost and simple way was developed to scalable prepare 3D hierarchical micro/nanostructured PANI. The possible formation mechanism, electrochemical performance, and the adsorption performance for dyes, for the first time, of the obtained superstructures were investigated and explored extensively.

2. Experimental

2.1. Materials

All chemicals including Aniline, Ammonium persulfate (APS), and hydrochloric acid (HCl) were purchased from Sinopharm group chemical reagent Co.Ltd and used as received. Acid Red G (ARG, $C_{20}H_{12}N_2Na_2O_7S_2$, MW 509, λ_{max} = 503 nm) and other typical dyes including negatively charged methyl orange (MO, $C_{14}H_{14}N_3NaO_3S$, MW 327, λ_{max} = 465 nm), direct grey D (DGD, $C_{24}H_{22}N_6NaO_5S$, MW 530, λ_{max} = 571 nm), acid fuchsine (AF, $C_{20}H_{17}N_3Na_2OS_3$, MW 586, λ_{max} = 525 nm), and positively charged rhodamiane B (RhB, $C_{20}H_6Br_4Na_2O_5$, MW 476, λ_{max} = 543 nm) and methylene blue (MB, $C_{18}H_{18}ClN_3S$, MW 320, λ_{max} = 663 nm) were commercial grade and recrystallized twice before used. The chemical structure of ARG is shown in Figure S1.

2.2. Syntheses of the PANI hierarchical micro/nanostructures

The PANI hierarchical micro/nanostructures were synthesized by simple adjusting the charging sequence *in situ* conventional chemical oxidative polymerization method. In a typical process, aniline (4.0 ml) was added into 200 ml deionized water under mechanical stirring at 0 °C. After stirring for 10 min, HCl (5 M, 10 mL) was added into the dispersion rapidly, and then followed by the pouring of an aqueous solution of APS (14.8 g) dissolved in HCl (0.25 M, 200 mL). After reaction for 12 h, the precipitate was filtered and washed with deionized water and acetone until the filtrate became colorless. The obtained product was dried at 50 °C for 24 h and labeled as CL-PANI. Control experiments were also conducted under the different polymerization conditions, as shown in Table S1.

2.3. Characterization

The morphologies of as-prepared products were characterized by a Gemini SEM 500 Field Emission Scanning Electron Microscope and a JFM-F200 Field Emission Transmission Electron Microscopy. Samples for SEM studies were prepared by 1–2 drops of dispersion onto the silicon wafer, and samples were dropped onto the carbon-coated copper grids for TEM studies. Fourier transform infrared spectroscopy (FT-IR) was performed on a Bruker, TENSOR37 infrared spectrometer with KBr pellets. UV-Vis spectroscopy of diluted PANI in ethanol dispersion was recorded on a UV2600, Shimadzu spectrophotometer. The crystal structures were determined on a Rigaku Dmax-RA with a scan rate of 4 deg min^{-1}. Nitrogen adsorption/desorption isotherm was measured by Builder SSA-4200 instrument using the Barrett-Joymer-Halenda (BJH) method.

2.4. Electrochemical experiment

Electrochemical measurements including cyclic voltammetry (CV), galvanostatic charge-discharge (GCD) and electrochemical impedance spectroscopy (EIS) were performed on a CHI 660D electrochemical work station in 1.0 M H_2SO_4 with a three-electrode cell, using Pt foil and Ag/AgCl (3.8 M KCl) as the counter and reference electrodes, respectively. The working electrode was prepared by mixing 70 wt% active material (PANI products), 20 wt% carbon black (super-P-Li) as conducting agent and 10 wt% binder (polyvinylidene difluoride, PVDF). The as-prepared slurry was pasted onto the carbon paper electrode (Aido Hengsheng Technolog co.Ltd, Tianjing, China) and dried at 60 °C for 24 h under vacuum. The used blank carbon paper electrode had a negligible electrochemical capacity compared with the as-prepared CL-PANI electrode (Figure S2). The mass loading for the active materials was around 1.0 mg cm^{-2} calculated with an Analysis balance (METTLER AE240).

2.5. Adsorption experiment

The adsorption experiment were investigated by shaking the mixture of ARG dye solution with the as-prepared PANI at various conditions like solution pH (1–11) (adjusted by 0.1 M HNO_3 or 0.1 M NaOH aqueous), adsorbent dosage (0.5–4 g L^{-1}), initial concentration of ARG (300–500 mg L^{-1}) and temperature (288 K-308 K). Then the suspension was collected by centrifugation and filtered using 0.45 μm filter membrane. In the regeneration experiment, the adsorbent was desorbed using 0.1 mol L^{-1} NaOH first for 5 min and then activated by 0.1 mol L^{-1} HNO_3 for another 5 min. The ARG concentration before and after adsorption was measured at λ = 503 nm by a UV-Vis spectrophotometer to evaluate the adsorption capacity of adsorbents. The adsorbed dye amount on per gram of adsorbent (Q_t (mg g^{-1})) in time *t*, the adsorption rate *R* (%), the kinetic models (pseudo-first-order, pseudo-second-order and Elovich mass transfer models) and adsorption isotherms (Langmuir, Freundlich and Temkin isotherm models) were calculated using Eqs. (S1-8) shown in Supporting Information.

3. Results and discussion

3.1. Morphology and structure of the CL-PANI

3.1.1. Morphology of CL-PANI

Fig. 1 shows the morphology of the as-prepared CL-PANI measured

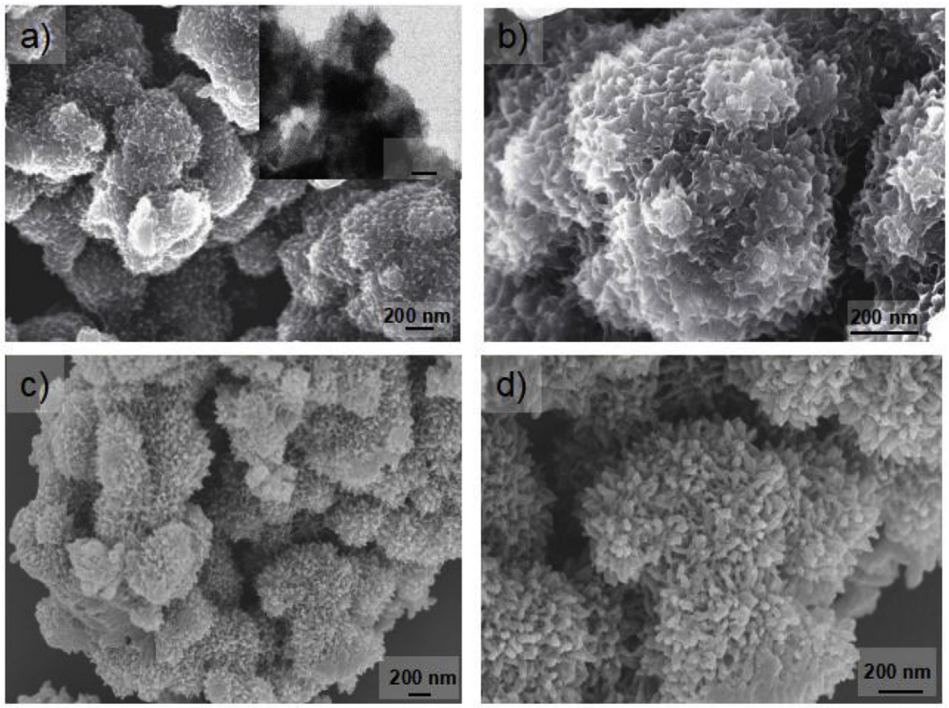

Fig. 1. FESEM images of the CL-PANI obtained after polymerization for 12 h under different area and magnifications without (a,b) and with (c,d) Au coating. The inset in (a) shows the TEM image of the as-prepared CL-PANI.

via FESEM and TEM. In the low-magnification FESEM images (Fig. 1a), it can be noted that the hierarchical micro/nanostructures of PANI have been successfully self-assembled *via* the simple polymerization method. The TEM image shown in Fig. 1a inset also reveals the hierarchical nature of the obtained morphology. During the SEM measurement process, it was found that these structures were easily deformed by the high energy of electron beam. Therefore, samples were coated with Au nanoparticles. As shown in Fig. 1c, CL-PANI presented highly quality 3D coral-like hierarchical micro/nanostructures. The high-magnification FESEM images shown in Fig. 1b demonstrated that the 3D hierarchical micro/nanostructures were composed of the well-defined short nanowires with ca.20 nm in diameter. Plenty mesoporous structures between the interconnected nanowires with Y-shape or V-shape were generated (Fig. 1b,d), which would be conducive to increasing the surface area of electrode/electrolyte and adsorbent/adsorbate interface [25].

3.1.2. Growth mechanism of the CL-PANI

Here, the CL-PANI was prepared *via* a regular conventional polymerization method but with simple adjustment of the charging sequence where aniline was added to deionized water firstly and the followed by the addition of acid and oxidant at 0 °C. The morphology of simple structured PANI (S-PANI) was therefore compared with that of the CL-PANI to study the effect of charging sequence. Normally, aniline was protonated completely firstly and then followed by the addition of oxidant for the synthesis of PANI with high molecular weight. It is known that PANI nanofiber formed simultaneously induced by concentrated protonated aniline salt, i.e. reactive aniline cation-radicals and then subsequent heterogeneous nucleation occurred on their surface [17]. That is believed to result in the non-directional growth of nanofibers and the precipitation of granules at a fast rate [26], as the SEM image shown in Fig. 2a. Here, coral-like hierarchical micro/nanostructures were obtained when concentrated aniline was added into the deionized water firstly and then followed by the addition of acid with high concentration and oxidant. We found that this simple change of charging sequence played the important role in the morphology of final PANI products. A likely explanation is that the concentration of protonated aniline salt is different in these two systems. Aniline could be protonated completely when it was added into the acid solution in the conventional polymerization system, while aniline (p*K*a value of 4.6) [27] would be protonated gradually due to the existence of concentration gradient in pH potential when high concentrated acid was added in the dispersion of aniline, which would generate the concentration gradient of protonated aniline. Concentration gradient has been proven to suppress crystal nucleation and here it might have a regulatory effect on the reaction kinetics for heterogeneous nucleation and directional growth of nanowires by limiting molecular mobility (Scheme 1) [28–31]. The detailed mechanism needs to be further studied.

It is well known that the morphology of PANI is strongly dependent on the reaction conditions like temperature, the mole ratio of APS to aniline ([APS]/[Ani]), concentration, the type of acid and so on [13,32]. Hence, different control experiments under different reaction conditions (Table S1) were carried out to investigate the mechanism responsible for the formation of 3D coral-like hierarchical structure. Fig. 2b and c shows the SEM images of PANI synthesized in different temperatures which is another factor affecting the reaction kinetics of PANI polymerization. It can be noted that the morphology of PANI-1 was irregular lumps while PANI-2 was irregular granular. Here, in the frozen reaction system under static condition without any addition of ionic strength or unfrozen agent like ethanol is not beneficial for the formation of nanowires. While heterogeneous nucleation with a fast rate under high temperature leads to the formation of irregular granular [14]. All of the other PANI products synthesized *via* different concentrations, different [APS]/[Ani] and different type of acids exhibit the 3D coral-like hierarchical structure (Figure S3,4,5), indicating that these changes had no significant influence on the formation of CL-PANI hierarchical structures. Based on the above morphology analysis, we speculated that the depressed reaction kinetics caused by the concentration gradient and low temperature in the unfrozen system may be the keys for the unique hierarchical structure of the CL-PANI.

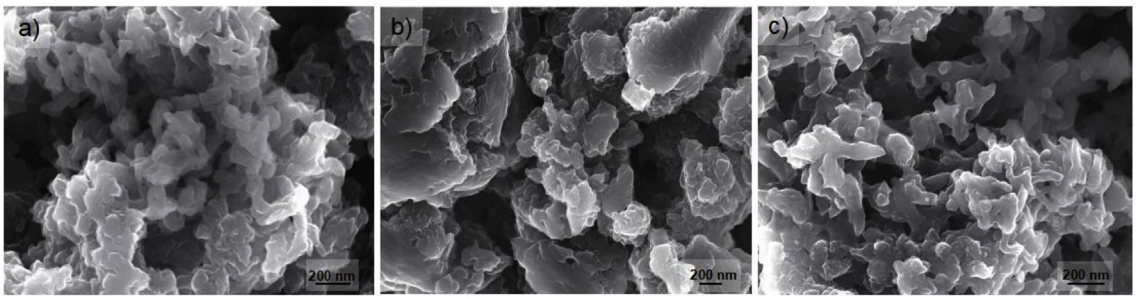

Fig. 2. FESEM images of PANI prepared under different conditions: (a) S-PANI (acid first); (b) PANI-1(-10 °C); (c) PANI-2 (25 °C).

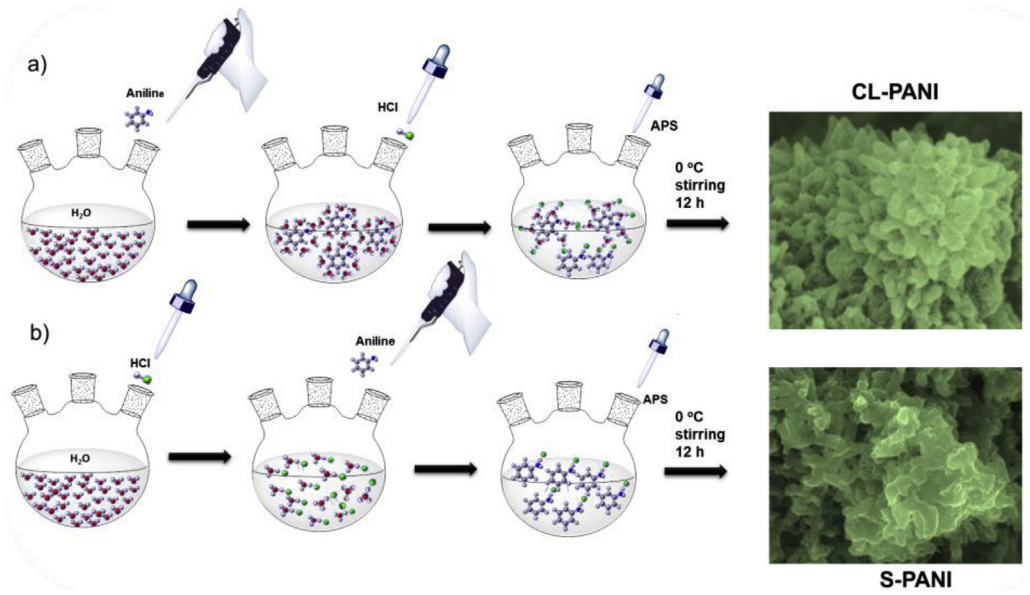

Scheme 1. The differences of the charging sequence at 0 °C between the CL-PANI and S-PANI prepared using the conventional chemical polymerization method.

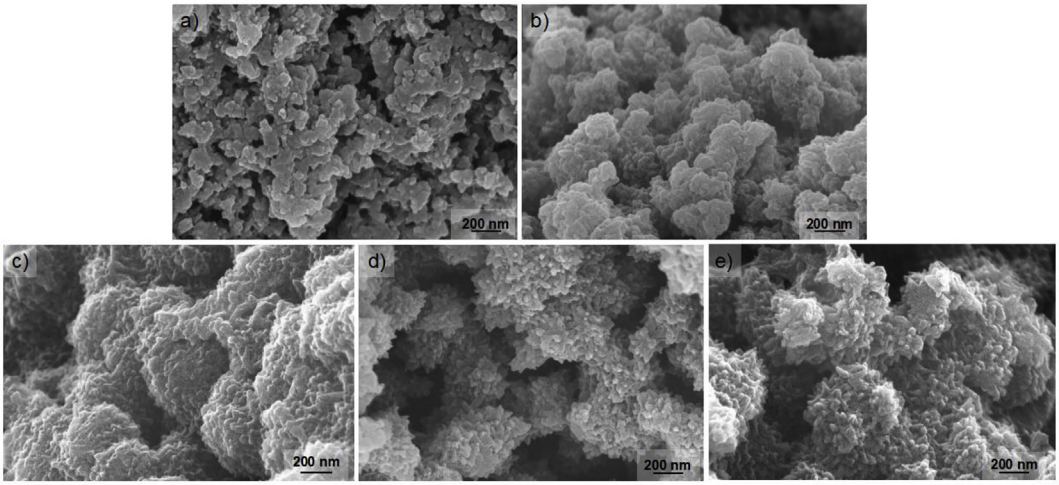

Fig. 3. Evolution of CL-PANI. SEM images showing CL-PANI collected at (a) 10 min, (b) 15 min, (c) 20 min, (d) 25 min, and (e) 30 min.

3.1.3. Evolution process of CL-PANI

The time-lapsed mechanistic studies were further carried out to monitor the evolution of the hierarchical morphology for CL-PANI. The polymerization process was quenched *via* rapid filtration after a certain time of growth. The formation process of CL-PANI could be divided into three stages. At the first stage, PANI product obtained when the reaction media changed from colorless to light blue at first 10 min shows no obvious morphology but with some nanoparticles which may be the intrinsic morphology for CL-PANI (Fig. 3a) [1]. At the second stage, i.e. after 15 min (Fig. 3b), a cluster of nanoparticles which further self-assembled into short nanowires after another 5 min can be seen (Fig. 3c). And at this stage, the color of the polymerization medium changed to green. When the polymerization time is extended to 25 min, i.e. the third stage, nanowires grew longer and the 3D coral-like hierarchical structure could be observed (Fig. 3d). Noticeably, the morphology of PANI product prepared at 30 min shown in Fig. 3e is similar to the final

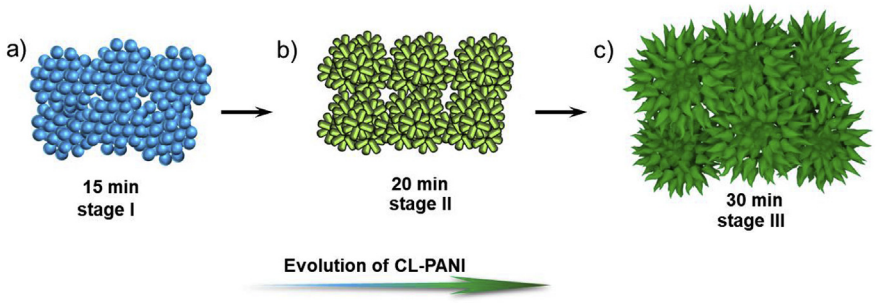

Scheme 2. Scheme image showing the possible evolution process of CL-PANI based on Fig. 3.

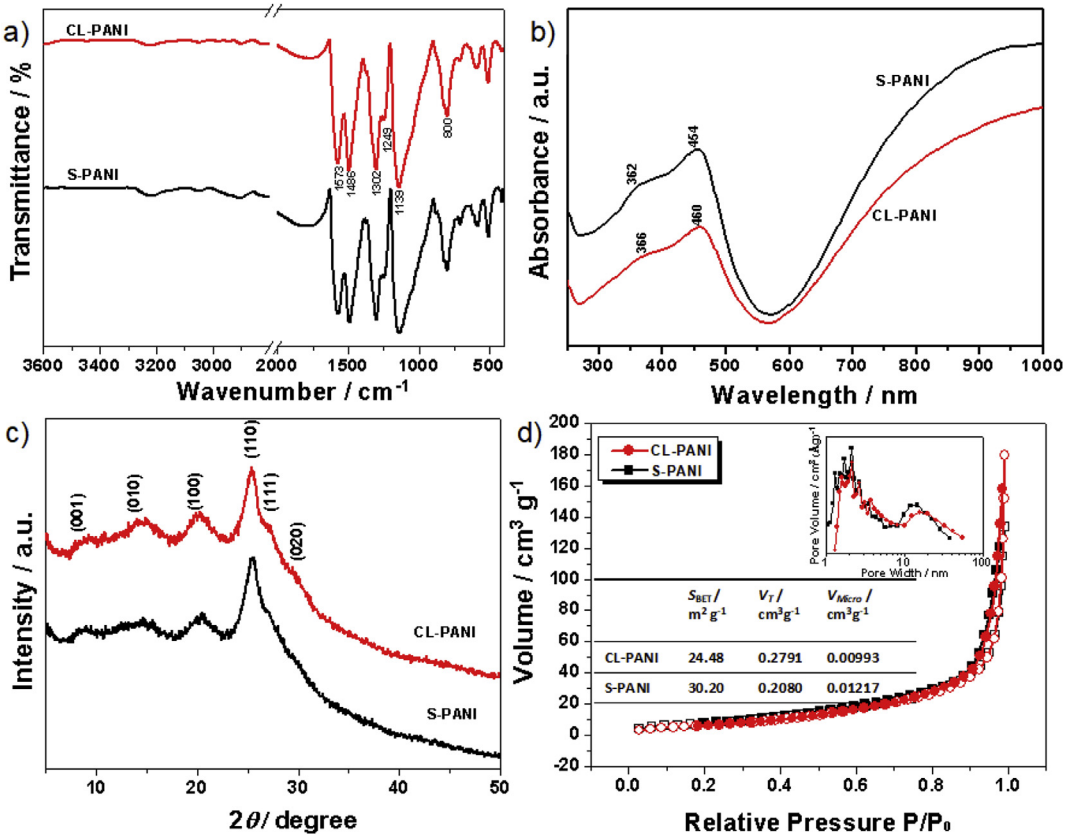

Fig. 4. (a) FT-IR, (b) UV-vis, (c) PXRD spectra and (d) N_2 adsorption-desorption isotherms of CL-PANI and S-PANI, with inset in d show the pore size distribution and textural properties of CL-PANI and S-PANI.

one obtained after 12 h. From these evolutional morphologies and the above mechanism analysis, we can speculate that nanoparticles may form firstly which is similar to Jadranka's observation that nanoparticles are the intrinsic morphology of self-assembled PANI [33] and then self-assembled into a cluster *via* heterogeneous nucleation at a depressed reaction kinetics (Scheme 2a). With the increase of reaction time, these nanoparticles further self-assembled into nanowires (Scheme 2b). The well-defined coral-like hierarchical structure, which is determined by the induced period [16], formed when reaction time is over 30 min (Scheme 2c). And in the later polymerization time, the oligomer chains grew to attain high molecular weights [16].

3.1.4. Structure and textural analysis of CL-PANI

The molecular structure of CL-PANI was then characterized by FT-IR, UV-Vis, and powder XRD spectra. Fig. 4a shows the FT-IR spectrum of CL-PANI. The main characteristic stretching vibrations of CL-PANI were located at 1573 cm^{-1} ($\nu_{C=C}$ for quinoid rings), 1486 cm^{-1} ($\nu_{C=C}$ for benzeniod rings), 1302 cm^{-1} (π-electron delocalization), 1249 cm^{-1} ($\nu_{C\text{-}N^{+}}$) and 1139 cm^{-1} ($\nu_{\text{-}NH=}^{+}$), respectively, which are typical for PANI in emeraldine salt (ES) state [34]. The UV-Vis spectrum of CL-PANI shown in Fig. 4b further confirms this structure, where three bands located at 366 nm, 460 nm and 1000 nm with a free tail extended to the IR region were observed. These peaks originated from the π-π*, polaron-π* and π-polaron band transitions, respectively, which are characteristic of the ES state of doped PANI [35]. S-PANI obtained *via* conventional polymerization method exhibited the similar FT-IR spectrum and same characteristic peak locations, but had the blue-shifted bands location in its UV-Vis spectrum compared with that of CL-PANI. The transitions at a longer wavelength in the UV-Vis spectrum indicated that CL-PANI molecule presented a better π-π stacking and a more extended chain conformation, which could be supported further by the XRD spectra. As shown in Fig. 4c, the main peaks of CL-PANI were located at 2θ values of 9.0, 14.7, 20.2, and 25.5° together with two shoulder peaks around 26.8 and 29.5°, which were assigned to the (001), (010), (100), (111) and (020) reflections of PANI, respectively [36]. The well-defined peaks indicated that CL-PANI was in

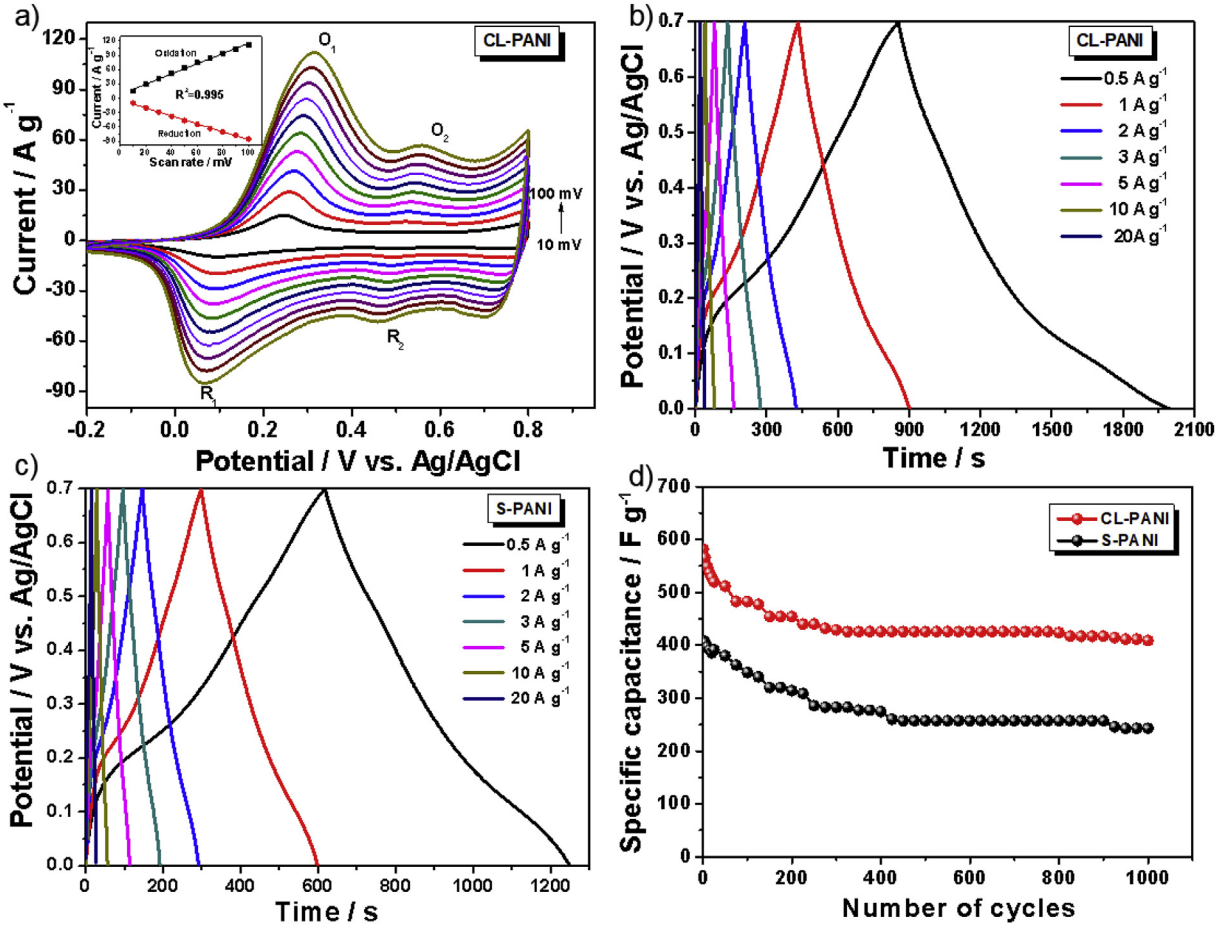

Fig. 5. (a) CV curves for the CL-PANI electrode at different potential scan rates: 10–100 mV s^{-1}, with inset-showing the relationships between the oxidation (O_1) and reduction (R_1) peak current vs. potential scan rate; GCD curves for the CL-PANI (b) and S-PANI (c) electrode at different current densities from 0.5 to 20 A g^{-1}; (d) cycling stability of CL-PANI and S-PANI electrode at a current density of 2 A g^{-1} 1.0 M H_2SO_4 was used as the electrolyte solution in all of the electrochemical measurements.

the form of a highly doped ES and exhibits good crystallinity [37]. Comparably, S-PANI showed the same peaks but with slight weaker intensity, especially the one around 26.8° which is corresponding to classical π-π stacking between aromatic rings [38]. The higher crystallinity is believed to improve the faradic redox reaction and benefit the mass transfer of charge and ions [14], endowing CL-PANI with an expected enhanced performance in the relevant area like electrochemical pseudocapacitance and adsorption capacity for some pollutants.

The N_2 adsorption-desorption study was then carried out to estimate the Brunauer-Emmett-Teller (BET) specific surface area (S_{BET}), total pore volume (V_T), and micropore volume (V_{Micro}) of CL-PANI. As shown in Fig. 4d, the isotherm of CL-PANI showed a typical Type-III nitrogen sorption behavior with a significant hysteretic loop showing at relative pressure $P/P_0 > 0.7$, which is characteristic of materials with larger mesoporous and macroporous [39]. The pore size distribution calculated from Barrett-Joyner-Halenda (BJH) shown in the inset revealed a bimodal distribution centered around 2.1 nm and 15.7 nm in the mesopore region (2–50 nm). As the discussion in SEM analysis, the unique Y-shaped or V-shaped nanowires units of hierarchical CL-PANI structure crossed each other and form these smaller mesopores. The calculated S_{BET} of CL-PANI was 24.48 $m^2 g^{-1}$, which is similar to the one obtained from other 3D urchin-like PANI [40]. Compared with S-PANI, CL-PANI exhibited a higher V_T value (0.2791 $cm^3 g^{-1}$), a lower V_{Micro} value (0.00993 $cm^3 g^{-1}$) and therefore a lower S_{BET}, which further supported the existence of plenty unique mesoporous structures in CL-PANI.

3.2. Electrochemical characterization

Like other reported PANI with hierarchical structure, CL-PANI prepared *via* the simple method with porous structure, high doping level and high crystallinity in this study is expected to have an improved electrochemical pseudocapacitance. Therefore, the electrochemical performance of CL-PANI as electrode was evaluated. Fig. 5a shows the CV curves of CL-PANI electrode at a scan rate ranging from 10 mV s^{-1} to 100 mV s^{-1}. Two pairs of redox peaks (O_1R_1 and O_2R_2) attributed to leucoemeraldine base (LEB)/emeraldine base (EB) and EB/pernigraniline (PA) transition of PANI, respectively, can be observed, indicating that the capacitance of CL-PANI mainly came from Faradaic reactions [41]. Besides, it can be noted that a liner dependence of the peak currents with the scan rates from the inset of Fig. 5a, suggesting that the electrochemical activity of the prepared CL-PANI electrode was a surface controlled process and CL-PANI had a very rapid current response on voltage reversal [41].

Galvanostatic charging-discharging (GCD) testes were then studied to evaluate the capacitance of CL-PANI at different current densities ranging from 0.5 to 20 A g^{-1} using a potential window 0–0.7 V versus Ag/AgCl [41–43]. C-PANI showed typical capacitance characteristics as displayed in the GCD curves of Fig. 5b. The specific capacitance is calculated as following:

$$C_m = \frac{I \times \Delta t}{\Delta V \times m}$$

where C_m (F g^{-1}) is the specific capacitance, I (A) is the discharge

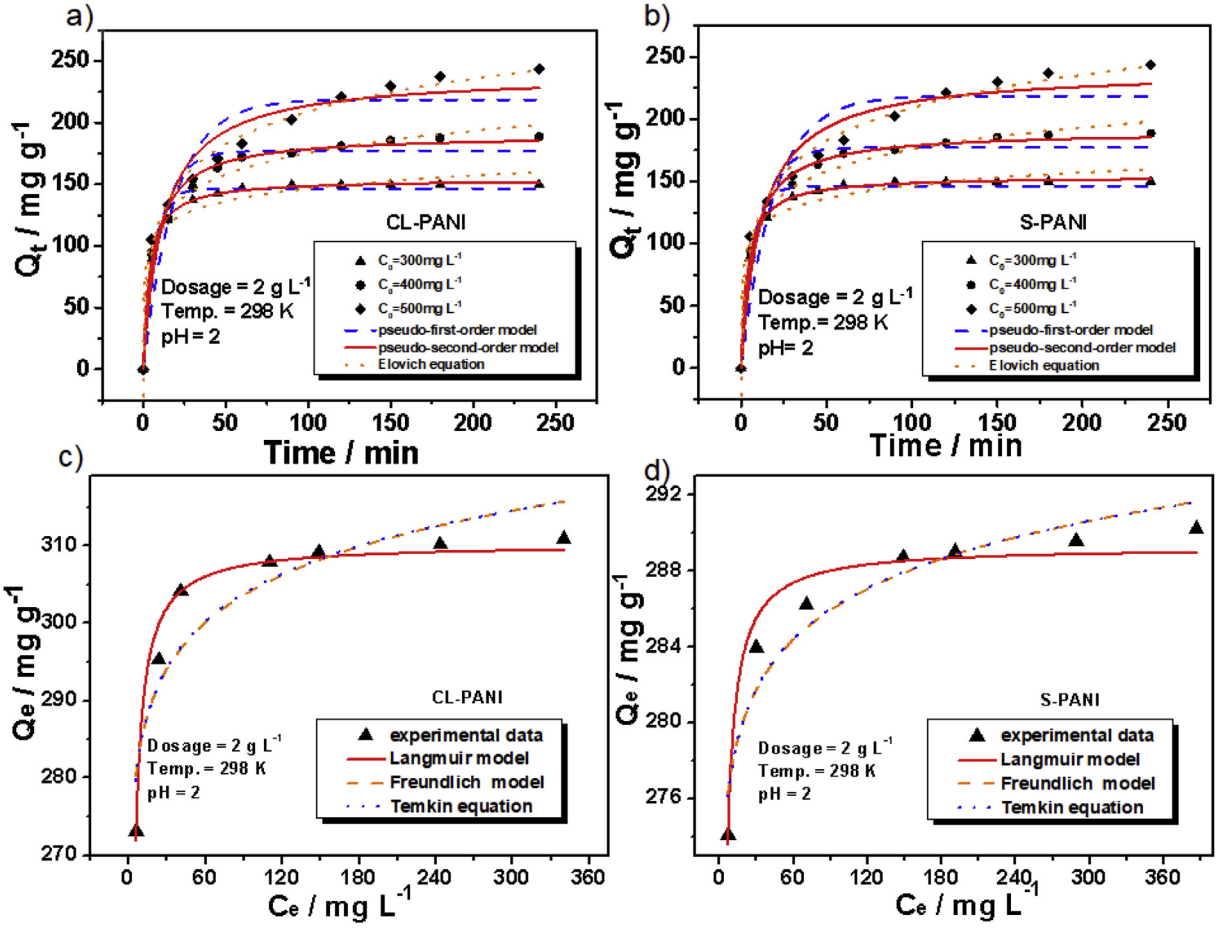

Fig. 6. Kinetics plots of ARG adsorption onto CL-PANI (a) and S-PANI (b) with initial concentrations of 300 mg L^{-1}, 400 mg L^{-1}, 500 mg L^{-1} fitting with pseudo-first-order, pseudo-second-order and Elovich models; adsorption isotherms for ARG adsorption onto CL-PANI (c) and S-PANI (d) at temperature of 298 K fitting with Langmuir, Freundlich and Temkin model.

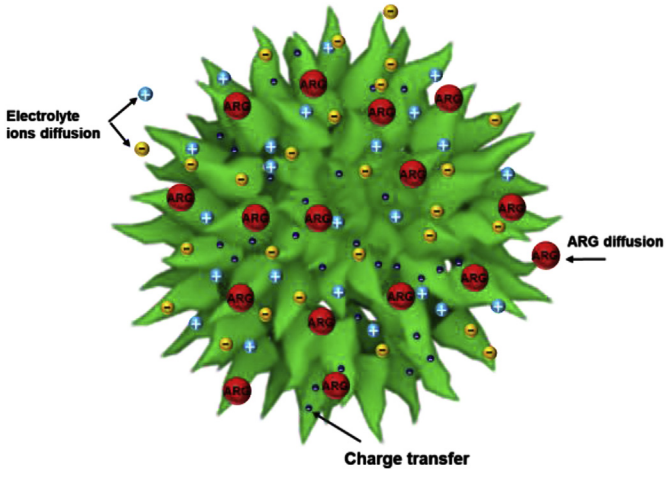

Fig. 7. Schematic image showing the diffusion of electrolyte ion and ARG ionion ion and charge transfer at the 3D hierarchical structure of CL-PANI.

current, Δt (s) is the discharge time, ΔV (V) is the potential change during discharge and m (g) is the mass of the active material in each electrode. The specific capacitance of CL-PANI could reach as high as 817 F g^{-1} at discharge current density of 0.5 A g^{-1}, while the specific capacitance of S-PANI was 452 F g^{-1} (Fig. 5c). This may be because of the smaller diameters of short nanowires in 3D coral like hierarchical structure providing an optimized ionic transport pathway, its unique mesoporous structure providing larger specific surface area of electrode/electrolyte interface and its high doping level and good crystallinity obenefiting charge transfers, endowing CL-PANI with the excellent pseudocapacity at lower current density. The specific capacitance remained at 540 F g^{-1} when the current density was increased to 20 A g^{-1}, which was still larger than that of S-PANI (Figure S6a), indicating that CL-PANI electrode had a good rate capability at a large current density which is important for supercapacitor electrode providing high power density [44]. The Nyquist plots of CL-PANI and S-PANI electrodes both showed a straight line at the low frequency which indicated that both of samples exhibited an ideal capacitive behavior, and an inconspicuous semicircle at the high frequency which is related to the low charge transfer resistance (Figure S6b). The slop of CL-PANI electrode was much steeper than that of S-PANI electrode, suggesting that CL-PANI electrode was more capacitive.

The cycling stability was further investigated in 1.0 M H_2SO_4 aqueous electrolyte by 1000 consecutive charge-discharge cycles at a current density of 2 A g^{-1}. As shown in Fig. 5d, the capacitance retention of CL-PANI kept 70.4% of its initial one after 1000 cycles, while S-PANI kept only 59.4% of its initial capacitance. The better stability of CL-PANI is expected to come from its porous structure which could accommodate the volume variation during the charge/discharge process [45]. To sum up, CL-PANI showed an enhanced electrochemical performance due to its unique 3D hierarchical structure and good crystallinity.

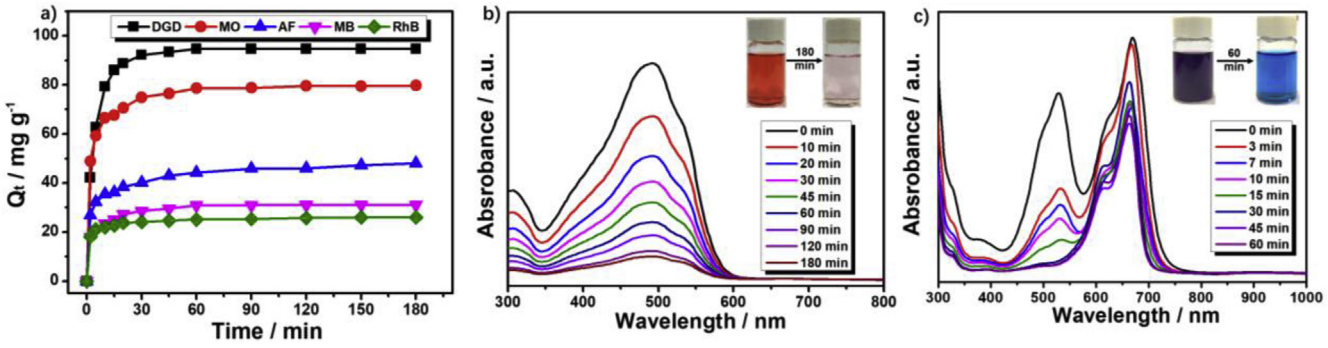

Fig. 8. (a) Different dyes removal by CL-PANI at pH of 6.5 and 25 °C (C_0 = 200 ppm); (b) removal ARG + MO + AF anionic dyes mixture solution (C_{ARG} = 100 ppm, C_{MO} = 100 ppm, C_{AF} = 100 ppm) by PANI-NFs/SD at pH of 6.5 and 25 °C; and (c) selective removal of ARG from ARG + MB dyes mixture solution (C_{ARG} = 100 ppm, C_{MB} = 100 ppm) by CL-PANI at pH of 6.5 and 25 °C, with inset showing the corresponding photo image before and after dyes removal.

3.3. Batch adsorption studies

3.3.1. Adsorption performance

To date, micro/nanostructured PANI has been demonstrated to be a promising material for highly effective collection of dyes and metal ions [19–24]. However, the 3D hierarchical PANI micro/nanostructures have not been explored in this area. Here, the CL-PANI has shown improved performance in supercapacitor due to its unique hierarchical morphology and chemical structure. It is also expected that CL-PANI would show enhanced adsorption performance for the removal of toxic pollutants from water. Therefore, Acid Red G, a typical azo anionic dye, was selected to investigate CL-PANI's adsorption performance. CL-PANI exhibited a higher ARG removal efficiency of 99% (C_0 = 300 mg L^{-1}) at a pH value below 7 (Figure S7a), indicating that ARG can be easily adsorbed onto CL-PANI in neutral and acid solution. The possible reason is that CL-PANI had a pH_{PZC} (the pH value of zero charge) value of 6.8 and CL-PANI was positively charged below this value, making ARG anionic dye molecules being attracted by electrostatic interaction. The adsorption of ARG as a function of CL-PANI dosage is shown in Figure S7b. With the increase of dosage, the adsorption efficiency increased, while the adsorption capacity decreased due to the unsaturation of adsorption site and particle interactions resulting from high adsorbent dose [46]. And the suitable dosage of CL-PANI for ARG removal was found to be 2.0 g L^{-1} (Figure S7b). Fig. 6a shows the adsorption kinetics fitting curves of CL-PANI using the pseudo-first-order, pseudo-second-order and Elovich models and the determined value of the kinetics parameters are listed in Table S2 [47]. It can be noted that the calculated value of Q_e and the correlation coefficients (R^2) from pseudo-second-order model fit better than others, indicating the chemisorption involved in the adsorption process of ARG dyes onto CL-PANI. S-PANI exhibited the same adsorption kinetics behaviors, but had a relatively slow adsorption rate and adsorption capacity in a certain time (Fig. 6b and Table S2). The adsorption isotherm behaviors of CL-PANI and S-PANI at 298 K were therefore fitted using Langmuir, Freundlich and Temkin isotherm models [48]. The fitting curves are shown in Fig. 6c and d and the calculated parameter values are listed in Table S3. It can be seen that the adsorption of ARG onto both PANI samples were well correlated by Langmuir isotherm which gives a higher R^2 value, suggesting that the adsorption process was a monolayer adsorption. And the maximum adsorption amount of PANI onto CL-PANI and S-PANI at 298 K derived the Langmuir model were 310.2 mg g^{-1} and 289.3 mg g^{-1}, respectively. The obtained results revealed that CL-PANI also presented an enhanced adsorption performance for ARG removal due to its unique 3D hierarchical morphology, as the scheme shown in Fig. 7. The comparison of the adsorption performance of CL-PANI with those of other micro/nanstructured conducting polymer adsorbents for anionic dye removal is listed in Table S4. It can be observed that anionic dye adsorption capacity of CL-PANI is outstanding higher than most of the reported micro/nanostructured conducting polymer. Therefore, it can be concluded that CL-PANI is a promising adsorbent for the removal of azo anionic dyes from industrial wastewater.

3.3.2. Selective dye absorption

Other typical dyes including anionic dyes (MO, DGD, AF) and cationic dyes (MB, RhB) were chosen to further study the adsorption performance of CL-PANI. As shown in Fig. 8a, CL-PANI showed a better adsorption performance on all anionic dyes (MO, DGD, AF) than cationic dyes (MB, RhB) at the pH of 6.5. This may because that CL-PANI was still positively charged with a pH_{pzc} of 6.8, therefore allowing anionic dyes easier been absorbed through the electrostatic attraction than cationic dyes. It indicated that C-PANI showed a selective adsorption for anionic dyes. Therefore, a mixture of multiple dye mixtures instead of a single model dye molecule, including dyes with same charge (ARG + MO + AF) and different charge (ARG + MB), were further chosen to study the adsorption performance of CL-PANI. The time-dependent UV-Vis adsorption spectra shown in Fig. 8b indicated that the anionic dyes mixture were almost removed within 180 min, while the spectra shown in Fig. 8c suggested that ARG was completely removed after 30 min and the concentration of MB in the solution was still high after 60 min. These results demonstrated that CL-PANI could selectively remove anionic dyes from mixture solution or wastewater.

3.3.3. Regeneration and reusability of CL-PANI

One of the important factors for adsorbents is their regeneration and reusability, which will make adsorption process cost-effective. Twenty consecutive adsorption-desorption cycles were therefore carried out to evaluate the reusability of CL-PANI for ARG (150 mg L^{-1}). As shown in Figure S8, the removal efficiency of ARG dye was 93.38% in the first regeneration after adsorption for 1 h. And after adsorption-desorption for 10 cycles, the value was still higher than 80%. The slight decrease in the removal efficiency during these 10 cycles may be due to the incomplete desorption of ARG on CL-PANI. After 18 cycles, the adsorption capacity started to decrease dramatically to 66%, which may be due to the breakage of the polymer chains by the repeated doping/dedoping cycles during the regeneration process. Nevertheless, this result indicated that the as-prepared CL-PANI was an efficient reusable adsorbent that can be easily generated by the treatment of weak acid and base.

4. Conclusion

In this study, an easy and low-cost approach for scalable synthesizing coral-like 3D hierarchical PANI micro/nanostructures (CL-PANI) was developed. Changing charging sequence was considered to be an effective way to generate concentration gradient of protonated aniline at the lower temperature, which can suppress the reaction kinetics for the formation of hierarchical structure of CL-PANI. Nanoparticles were

deduced to be intrinsic morphology of self-assembled CL-PANI in the time-lapsed evolution mechanistic studies. The CL-PANI possessed unique mesoporous and higher crystallinity, making it a promising material for supercapacitor's electrode and adsorption of toxic azo anionic dye. The as-prepared CL-PANI electrode showed an obvious improvement on the specific capacitance and cycling stability compared with S-PANI. The adsorption capacity of ARG dyes on CL-PANI was also larger than that on S-PANI. Therefore, CL-PANI is anticipated to have a great potential application for large-scale applications in both battery and adsorption areas.

Acknowledgements

The authors gratefully acknowledge China Postdoctoral Science Foundation (Grant No.2018M633489), the Natural Science Basic Research Plan in Shaanxi Province of China (Grant No.2018JQ5033), the Shaanxi Key research and development projects, China (Grant No. 2017SF-386), the Fundamental Research Funds for the Central Universities of China and the financial supports from the National Natural Science Foundation of China (Grant No.21307098).

Appendix A. Supplementary data

Supplementary data to this article can be found online at https://doi.org/10.1016/j.polymer.2018.12.037.

References

[1] N.R. Tanguy, M. Thompson, N. Yan, A review on advances in application of polyaniline for ammonia detection, Sensor. Actuator. B Chem. 257 (2018) 1011–1064.
[2] A. Eftekhari, L. Li, Y. Yang, Polyaniline supercapacitors, J. Power Sources 347 (2017) 86–107.
[3] F. Wolfart, B.M. Hryniewicz, M.S. Goes, C.M. Correa, R. Torresi, M. Minadeo, S.I.C. de Torresi, R.D. Oliveira, L.F. Marchesi, M. Vidotti, Conducting polymers revisited: applications in energy, electrochromism and molecular recognition, J. Solid State Electrochem. 21 (2017) 2489–2515.
[4] H. Zhang, R.L. Zong, Y.F. Zhu, Photocorrosion inhibition and photoactivity enhancement for Zinc Oxide via hybridization with monolayer polyaniline, J. Phys. Chem. C 113 (2009) 4605–4611.
[5] E.N. Zare, A. Motahari, M. Sillanpää, Nanoadsorbents based on conducting polymer nanocomposites with main focus on polyaniline and its derivatives for removal of heavy metal ions/dyes: a review, Environ. Res. 162 (2018) 173–195.
[6] C.O. Baker, X. Huang, W. Nelson, R.B. Kaner, Polyaniline nanofibers: broadening applications for conducting polymers, Chem. Soc. Rev. 46 (2017) 1510–1525.
[7] G. Wang, R. Vivek, J.Y. Wang, Polyaniline nanoparticles: synthesis, dispersion and biomedical applications, Mini-Reviews Org. Chem. 14 (2017) 56–64.
[8] D. Uppalapati, B.J. Boyd, S. Garg, J. Travas-Sejdic, D. Svirskis, Conducting polymers with defined micro- or nanostructures for drug delivery, Biomaterials 111 (2016) 149–162.
[9] H.P. Jia, Q. Huang, Y.K. Zhen, D. Neo, Z.W. Xing, Q. Wang, Scalable synthesis of urchin- and flowerlike hierarchical NiO microspheres and their electrochemical property for lithium storage, ACS Appl. Mater. Interfaces 5 (2013) 6292–6299.
[10] Y. Zhu, D. Hu, M.X. Wan, L. Jiang, Y. Wei, Conducting and superhydrophobic rambutan-like hollow spheres of polyaniline, Adv. Mater. 19 (2007) 2092–2096.
[11] Y. Zhu, J. Li, M. Wan, L. Jiang, 3D-boxlike polyaniline microstructures with superhydrophobic and high-crystalline properties, Polymer 49 (2008) 3419–3423.
[12] Z. Ying, J. Li, M. Wan, J. Lei, Superhydrophobic 3D microstructures assembled from 1D nanofibers of polyaniline, Macromol. Rapid Commun. 29 (2008) 239–243.
[13] Z. Zhou, J. Wang, Z. Wang, F. Zhang, Self-assembly of polyaniline nanowires into polyaniline microspheres, Mater. Lett. 65 (2011) 2311–2314.
[14] X. Wang, M. Xu, Y. Fu, S. Wang, T. Yang, K. Jiao, A highly conductive and hierarchical PANI micro/nanostructure and its supercapacitor application, Electrochim. Acta 222 (2016) 701–708.
[15] Z. Zhang, J. Deng, L. Yu, M. Wan, Chrysanthemum flower-like constructed polyaniline nanofibers synthesized by adding inorganic salts as additives, Synth. Met. 158 (2008) 712–716.
[16] X. Zhang, H.S. Kolla, X. Wang, K. Raja, S.K. Manohar, Fibrillar growth in polyaniline, Adv. Funct. Mater. 16 (2006) 1145–1152.
[17] N.R. Chiou, C. Lu, J. Guan, L.J. Lee, A.J. Epstein, Growth and alignment of polyaniline nanofibres with superhydrophobic, superhydrophilic and other properties, Nat. Nanotechnol. 2 (2007) 354–357.
[18] G. Mazzone, M. Vittori Antisari, Nucleation of crystalline phases in plastically deformed amorphous NiZr, J. Appl. Phys. 77 (1995) 5020–5025.
[19] M. Bhaumik, H.J. Choi, R.I. McCrindle, A. Maity, Composite nanofibers prepared from metallic iron nanoparticles and polyaniline: high performance for water treatment applications, J. Colloid Interface Sci. 425 (2014) 75–82.
[20] V. Sharma, P. Rekha, P. Mohanty, Nanoporous hypercrosslinked polyaniline: an efficient adsorbent for the adsorptive removal of cationic and anionic dyes, J. Mol. Liq. 222 (2016) 1091–1100.
[21] L. Ai, J. Jiang, R. Zhang, Uniform polyaniline microspheres: a novel adsorbent for dye removal from aqueous solution, Synth. Met. 160 (2010) 762–767.
[22] J. Feng, J. Li, W. Lv, H. Xu, H. Yang, W. Yan, Synthesis of polypyrrole nano-fibers with hierarchical structure and its adsorption property of Acid Red G from aqueous solution, Synth. Met. 191 (2014) 66–73.
[23] M. Bhaumik, R. McCrindle, A. Maity, Efficient removal of Congo red from aqueous solutions by adsorption onto interconnected polypyrrole-polyaniline nanofibres, Chem. Eng. J. 228 (2013) 506–515.
[24] M. Bhaumik, R.I. McCrindle, A. Maity, S. Agarwal, V.K. Gupta, Polyaniline nanofibers as highly effective re-usable adsorbent for removal of reactive black 5 from aqueous solutions, J. Colloid Interface Sci. 466 (2016) 442–451.
[25] X.S. Du, C.F. Zhou, G.T. Wang, Y.W. Mai, Novel solid-state and template-free synthesis of branched polyaniline nanofibers, Chem.Mater. 20 (2008) 3806–3808.
[26] S.P. Surwade, N. Manohar, S.K. Manohar, Origin of bulk nanoscale morphology in conducting polymers, Macromolecules 42 (2009) 1792–1795.
[27] J. Stejskal, I. Sapurina, M. Trchová, E.N. Konyushenko, Oxidation of aniline: polyaniline granules, nanotubes, and oligoaniline microspheres, Macromolecules 41 (2012) 3530–3536.
[28] F. Hodaj, P.J. Desré, Effect of a sharp gradient of concentration on nucleation of intermetallics at interfaces between polycrystalline layers, Acta Mater. 44 (1996) 4485–4490.
[29] P.J. Desré, A.R. Yavari, Suppression of crystal nucleation in amorphous layers with sharp concentration gradients, Phys. Rev. Lett. 64 (1990) 1533–1536.
[30] M. Ibrahim, Z. Balogh-Michels, P. Stender, D. Baither, G. Schmitz, Nucleation controlled reaction of Cu3Si in the field of sharp concentration gradient, Acta Mater. 112 (2016) 315–325.
[31] P. Yi, M.L. Falk, T.P. Weihs, Suppression of homogeneous crystal nucleation of the NiAl intermetallic by a composition gradient: a molecular dynamics study, J. Chem. Phys. 146 (2017) 81–134.
[32] J. Stejskal, A. Riede, D. Hlavatá, J. Prokeš, M. Helmstedt, P. Holler, The effect of polymerization temperature on molecular weight, crystallinity, and electrical conductivity of polyaniline, Synth. Met. 96 (1998) 55–61.
[33] C. Laslau, Z.D. Zujovic, J.T. Sejdic, Polyaniline nanotube self-assembly: the stage of granular agglomeration on nanorod templates, Macromol. Rapid Commun. 30 (2009) 1663–1668.
[34] P. Colomban, A. Gruger, A. Novak, A. Régis, Infrared and Raman study of polyaniline part I. Hydrogen bonding and electronic mobility in emeraldine salts, J. Mol. Struct. 317 (1994) 261–271.
[35] Y. Xia, J.M. Wiesinger, A.G. MacDiarmid, A.J. Epstein, Camphorsulfonic acid fully doped polyaniline emeraldine salt: conformations in different solvents studied by an Ultraviolet/Visible/Near-Infrared spectroscopic method, Chem. Mater. 7 (1995) 443–445.
[36] J.P. Pouget, M.E. Jozefowicz, A.J. Epstein, X. Tang, A.G. MacDiarmid, X-ray Structure of polyaniline, Macromolecules 24 (1991) 779–789.
[37] Z. Zhang, J. Deng, J. Shen, M. Wan, Z. Chen, Chemical one step method to prepare polyaniline nanofibers with electromagnetic function, Macromol. Rapid Commun. 28 (2010) 585–590.
[38] Y. Wang, J. Liu, H.D. Tran, M. Mecklenburg, X.N. Guan, A.Z. Stieg, B.C. Regan, D.C. Martin, R.B. Kaner, Morphological and dimensional control via hierarchical assembly of doped oligoaniline single crystals, J. Am. Chem. Soc. 134 (2012) 9251–9262.
[39] G. Li, L. Guan, Y. Liu, C. Liu, Template-free solvothermal synthesis of 3D hierarchical nanostructured boehmite assembled by nanosheets, J. Phys. Chem. Solid. 73 (2012) 1055–1060.
[40] M.J. Kim, Y.D. Liu, H.J. Choi, Urchin-like polyaniline microspheres fabricated from self-assembly of polyaniline nanowires and their electro-responsive characteristics, Chem. Eng. J. 235 (2014) 186–190.
[41] J. Xu, K. Wang, S.Z. Zu, B.H. Han, Z. Wei, Hierarchical nanocomposites of polyaniline nanowire arrays on graphene oxide sheets with synergistic effect for energy storage, ACS Nano 4 (2010) 5019.
[42] K. Wang, J. Huang, Z. Wei, Conducting polyaniline nanowire arrays for high performance supercapacitors, J. Phys. Chem. C 114 (2010) 8062–8067.
[43] M. Xue, F. Li, J. Zhu, H. Song, M. Zhang, T. Cao, Structure-based enhanced capacitance: in situ growth of highly ordered polyaniline nanorods on reduced graphene oxide patterns, Adv. Funct. Mater. 22 (2012) 1284–1290.
[44] X. Peng, K. Huo, J. Fu, X. Zhang, B. Gao, P.K. Chu, Coaxial PANI/TiN/PANI nanotube arrays for high-performance supercapacitor electrodes, Chem. Commun. 49 (2013) 10172–10174.
[45] L. Mai, Q. An, Q. Wei, J. Fei, P. Zhang, X. Xu, Y. Zhao, M. Yan, W. Wen, L. Xu, Nanoflakes-assembled three-dimensional hollow-porous V_2O_5 as lithium storage cathodes with high-rate capacity, Small 10 (2014) 3032–3037.
[46] M. Ozacar, I.A. Sengil, Adsorption of metal complex dyes from aqueous solutions by pine sawdust, Bioresour. Technol. 96 (2005) 791–795.
[47] W.S. Wan Ngah, M.A.K.M. Hanafiah, Removal of heavy metal ions from wastewater by chemically modified plant wastes as adsorbents: a review, Bioresour. Technol. 99 (2008) 3935–3948.
[48] S.Y. Yoon, C.G. Lee, J.A. Park, J.H. Kim, S.B. Kim, S.H. Lee, J.W. Choi, Kinetic, equilibrium and thermodynamic studies for phosphate adsorption to magnetic iron oxide nanoparticles, Chem. Eng. J. 236 (2014) 341–347.